Study of Laser Metal Deposition (LMD) as a manufacturing technique in Automotive Industry

Ramalho, F.Q.[1] [0000-0003-3359-9681], Alves, M.L.[1] [0000-0002-5025-950X], Correia, M.S.[1, 2] [0000-0002-2176-6289], Vilhena, L.M.[2] [0000-0001-9592-3120], Ramalho, A.[2] [0000-0001-7004-2212]

[1] School of Technology and Management, Polytechnic Institute of Leiria, Leiria, Portugal
[2] Centre for Mechanical Engineering, Materials and Processes, University of Coimbra Coimbra, Portugal

Abstract. The last few decades in the automotive industry have been marked by a heavy concern with the environment, saving energy and reducing material wastage, while aiming to maintain good mechanical properties, essential in the components usage. Additive manufacturing (AM) techniques present themselves as a viable option in the matter, with Laser Metal Deposition (LMD), rising as one of the most promising techniques within this category, capable of producing near-net shape components, with a layer upon layer construction of three-dimensional solid parts from a 3D CAD model, with good mechanical properties and acceptable surface finishing. Laser Metal Deposition is a relatively recent technique, which is made noticeable by the lack of clarification about the influence of several parameters in the final components characteristics, ultimately leading to a scarce availability of the process in the market. This paper aims to clarify and evaluate, how LMD produced parts can suit the automotive industry, by measuring and analysing their behaviour under several mechanical tests. These mechanical tests have specific focus on wear and abrasion behaviour, as well as elastic properties determination, as these are the characteristics that allow a better overview over the expected performance of LMD components for automotive applications.

Keywords: Laser Metal Deposition, Additive Manufacturing, Automotive Industry.

1 Introduction

In the process of researching and developing better and more efficient manufacturing techniques, car manufactures invest significantly large quantities of money and time, which contributed to the development and perfecting of new and undeveloped manufacturing techniques and the manufacturing of components with good mechanical properties, allying with less energy consumption and less material wastage.

Additive manufacturing techniques rise as one of the most promising type of processes, since these allow the construction of components through an additive perspective, opposed to the more conventional ones with subtractive nature.

Within additive manufacturing techniques, Laser Metal Deposition (LMD) stands out as one of the main types of additive manufacturing when using metal as a deposition material, which is a key factor on the automotive industry, offering significant energy saving, almost null material waste, lower productions time and good reproducibility.

LMD is a technique capable of producing near-net shape metallic components with good mechanical properties, standing on the good adhesion between layers.

The biggest limitations of the technique stand on the poor surface finishing, which can be corrected with additional processing, and also the somewhat low resolution, since the layer thickness is dependent of the laser beam diameter.

This metallic additive manufacturing process is capable of a layer upon layer 3D part construction, using a high-power laser beam to achieve the fusion of a metallic material, which feeds in the form of either powder or wire through a nozzle, directly into a substrate of metallic nature [1].

Figure 1 (left) illustrates the deposition process, with the laser beam and powder or wire feeding system, as well as the substrate where the layer is deposited.

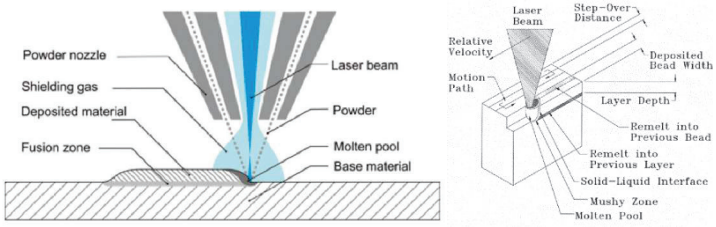

Fig. 1. Illustration of an LMD deposition process [2] (left) and schematic representation of layer deposition in LMD technology [3] (right).

The deposition process is made directly into a surface where a molten pool exists, allowing adhesion between layers through the surface tension, since the metal which is deposited in liquid form is held in place by the already solidified layers that exist on the periphery of the molten pool. This effect also allows the deposition of layers in virtually every direction wanted, including overhead depositions. The morphology of the molten pool area is illustrated on figure 1 (right) [3].

The successive vertical layer deposition creates an uneven cooling process of the several layers, which means the mechanical properties of the deposited material can vary throughout the components, since each layer cooling process is distinct from the others [4].

The cooling process can also be influenced by the vertical and horizontal overlap applied between the layers, which also influence the dimensions of the layers and the adhesion between them, and might introduce defects into the final component such as cracks or gaps [5].

The process often uses an inert gas, such as argon, helium or nitrogen that involves the molten pool, preventing oxidation of the parts.

For this the mechanical properties of components produced by LMD process are usually higher than the ones obtained through other conventional processes.

1.1 Powder and wire LMD

The powder LMD was the first type of LMD to be produced and it is slightly more advanced and established then wire LMD, mainly because it offers a more controlled and refined deposition process, with the possibility of robotic control, a much lower dilution rate between the deposited material and the substrate (5% against 20% verified on the wire variety), ending up on a much more refined microstructure due to a more controllable and constant deposition rate [6]. Another advantageous aspect is that the available metallic powder range is much broader than the range of metallic wires.

The downsides of powder LMD are often related to the powder manufacturing processes, which introduce higher costs and bigger health concerns due to the toxicity that the processes generate [7].

Wire LMD on the other hand, is usually a cheaper process to implement and run, and the complexity of the equipment is often lower, is capable of applying high deposition rates without influencing the porosity of the deposited layers and the material usage efficiency is near 100% which is another desirable aspect of the wire variant [8].

However, wire LMD as some downsides, most of which are related to the deposition process itself. The fact that the feed material is on the form of a metallic wire introduces difficulties in its fusion, not being able to function properly under robotic control and encountering several geometrical barriers, which end up meaning that this variant is uncapable of depositing thin walls, overhangs and hollow structures [9].

The wire feeding process is not able to maintain a clean and constant stream of wire to the laser focal zone, promoting some defects on the final components, however is significantly simpler to conduct when compared to the powder manufacturing techniques. It represents less cost and almost eliminates the health concerns present on the powder materials, even with an available range of metallic wire materials much more reduced.

2 Materials and methods

2.1 Equipment and material

Given the main goals of this work both powder and wire LMD components were used in order to analyse the feasibility of the process under certain production conditions, but also to achieve data that allows a distinction between the wire and powder variants of this process.

Regarding the powder LMD components, these were produced by IK4-Tekniker, on their facilities, using a 2.2 kW diode pumped continuous wave Rofin DY022 Nd:YAG laser, with the laser beam being guided towards the work area through a 0.6 mm diameter fiber and an optical head from Precitec. The powder was injected into the molten pool area, using a three-hole coaxial nozzle made by IK4-Tekniker. The movement of the laser head was implemented through a 6-axis ABB 4400 robot.

The powder was fed using a Sulzer Metco Twin-10C powder feeder, with a feed rate of 15 g/min and a translation speed of the laser head stock of 400 mm/min [1].

The several powder LMD components provided present different manufacturing layer shift heights since the distance between the deposition set (laser and powder feeder) and the molten pool was varied (0,3mm, 0,7mm, 0,8mm and 0,9mm), resulting in components with different characteristics. However, the values of distance between the deposition set and the molten pool do not directly correspond to the layer height itself, since this particular value is a result of the horizontal and vertical overlap, and the amount of deposited material.

The deposition material was Metco 42C Martensitic Stainless-Steel powder, which is identical to AISI 431 grade stainless steel and the substrate plate was C45E Carbon Steel, with 10 mm of thickness.

The wire LMD components were produced using roughly the same equipment, the laser power was lowered to 1,5kW, the translation speed was increased to 1200 mm/min and the wire feeding rate was of 3 m/min [1].

The wire LMD components, unlike the powder components, were produced using a fixed layer shift height of 0,9 mm.

The metallic wire used was made of AISI 316L austenitic stainless steel and the substrate plate material was also C45E Carbon Steel, with 10mm of thickness.

Both wire and powder components were manufactured using an overlap between consecutive layers of 40% of a single bead width, which in this case represented a value of 1,3mm. The deposition process of each layer consists of an external perimeter deposition followed by a zig-zag trajectory that ends up filling the inner section.

The components dimensions are shown in table 1, with the "*Px*" being the powder components and the "*Wx*" being the wire components.

Table 1. Powder and Wire LMD components dimensions (x, y, z).

Number identification	x [mm]	y [mm]	z [mm]	Deposition height [mm]
P1	12,55	28,05	78,80	0,3
P2	13,45	29,00	79,00	0,9
P3	11,10	27,00	77,50	0,8
P4	13,00	26,20	80,00	0,7
P5	13,00	27,50	78,70	0,8
W1	30,60	30,60	99,00	0,9
W2	30,60	30,90	60,00	0,9
W3	30,50	30,90	62,10	0,9
W4	30,30	30,90	37,90	0,9
W5	31,00	30,75	47,35	0,9

2.2 Mechanical test schedule

The planned mechanical tests that were conducted covered several aspects like the elastic properties of the components, surface characteristics and the friction and wear behaviour of the components under different conditions.

In order to achieve those results microhardness, density, impulse vibration tool analysis, friction and wear tests were performed.

The Vickers microhardness test was conducted under the ASTM E92 [13] standard, using a Shimadzu HMV-2 equipment, available on the School of Technology and Management of Polytechnic Institute of Leiria facilities, and was applied to both powder and wire LMD components, with the different layer characteristics. For this tests a load of 4,903 N was applied for 15 seconds on LMD surfaces.

Before carrying out the test, surface preparation were made by using a Struers Roto-Pol-21 and sandpaper disks with grits of 500, 800, 1200 and 2400.

In order to obtain a variation profile of the component's microhardness, the test was conducted in sets of 5 point with a 1mm distance between them, with a distance of 10mm between the first points of every set.

Through density testing the relation between a components mass and volume is achievable, which, alongside the data reference value for the material density in wrought shape, allows this comparative ratio.

This test was conducted under the Archimedes principle [13], using a Mettler Toledo AG204 scale.

The test consists in two weight measurements of the component, one in a dry condition and another in a submerged condition, which allows the calculation of the density of the component, through the equation (1).

$$d_{component} = \left(\frac{m_{dry}}{m_{dry} - m_{submerged}}\right) . d_{H_2O@T_{air}} \qquad (1)$$

Additionally, impulse excitation vibration tests were performed to achieve mechanical elastic properties such as Young's modulus, Shear modulus and the Poisson ratio.

Tests were conducted under the ASTM E1876-15 [14] standard.

The measurement of these fundamental resonant frequencies is made by mechanical exciting the component with a singular elastic strike using an impulse tool.

A transducer is then used to sense the resulting mechanical vibrations of the component, transforming them into an electric signal that is later analysed in order to obtain the fundamental resonant frequencies. The laboratorial apparatus is similar to the one presented in figure 2.

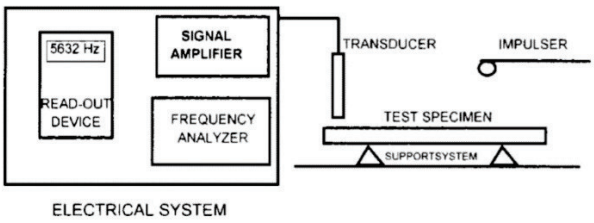

Fig. 2. Impulse excitation of vibration test equipment illustration [14].

Knowing the fundamental resonating frequency of the test subject, the following equations are then applied to achieve the aforementioned mechanical properties, namely the values of Young Modulus (E) and the Poisson ratio (μ).

$$E = 0{,}9465.\left(\frac{m_f^2}{b}\right).\left(\frac{L^3}{t^3}\right).T_1 \quad (2)$$

$$T_1 = 1 + 6{,}585.(1 + 0{,}0752.\mu + 0{,}8109.\mu^2).(\tfrac{t}{L})^2 - 0{,}868.\left(\frac{t}{L}\right)^4 - \left[\frac{8{,}340.(1+0{,}2023.\mu+2{,}173.\mu^2).(\frac{t}{L})^4}{1{,}000+6{,}338.(1+0{,}1408.\mu+1{,}536.\mu^2).(\frac{t}{L})^2}\right] \quad (3)$$

$$\mu = \left(\frac{E}{2.G}\right) - 1 \quad (4)$$

This test was conducted on the ICEMS – University of Coimbra homemade facilities. Both powder and the wire LMD were tested, both specimens with a layer height of 0,9mm.

The final destructive conducted test was the wear test, which is capable of offering a clearer idea of how a material behaves under specific environmental conditions, with the possibility to reproduce operating conditions such as temperature, fluid interactions, and direction of wear, amongst others.

The selected wear test had a reciprocating nature, allowing a variation in the amplitude of movement, sliding speed and in the normal load value, which ends up giving the possibility to emulate several test conditions that better characterize a real application of a component produced [15].

This test was performed using the ICEMS – University of Coimbra homemade reciprocating tribometer, and although it does not follow any specific standard, it is capable of simulating real conditions, allowing an evaluation of contact wear in both materials under testing.

The used geometry of contact was a ball to plane, being the ball (7) a zirconium sphere with 10 mm of radius, assembled in the moving stage (2), which is in permanent contact with the stationary horizontal plane (4), in the form of LMD components (Figure 3). The normal load is applied by a spindle-spring (5) which is supported by the normal load cell (1), that measures the normal load applied, which was 3, 5 and 7 N. A harmonic wave generated by an eccentric-and-rod mechanism set with stroke length of 2 mm and frequency of 3 Hz imposes the referred reciprocating movement of the upper sphere carrier. The LMD components were placed in the holder connected to a ball linear bearing slider in order to allow movement in the direction of the sliding reciprocating motion. The stationary load cell (3) is used to equilibrate the lower specimen holder attaining the friction force values along the test.

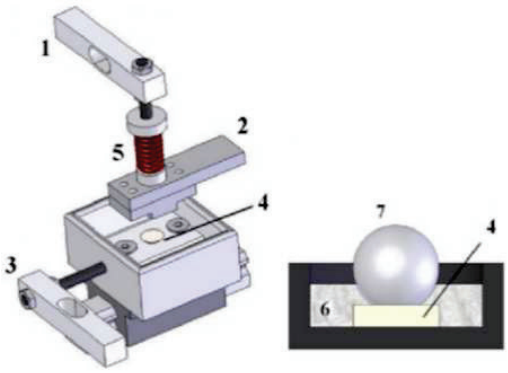

Fig. 3. Wear testing apparatus [15].

Result analysis on the stationary plane side (LMD samples) is made by measuring the area of the wear track and by integration it over the wear track length, obtaining the volume that was stripped away from the surface.

The results regarding the sphere are assessed by measuring directly its diameter. The measurement of the diameter was performed in two orthogonal directions, one along the relative motion direction and another in the perpendicular direction, and then using these two values to calculate the average radius (r) of the ball wear scar. Combining this average radius (r) and the original ball radius (R), it is then possible to obtain the depth (h) and volume (V) of the ball wear scar created during the test, by using equations (5) and (6). Finally, and using the depth and volume of the wear track, it is then possible to calculate the wear rate (k), using equation (7), where F is the normal force and L the sliding distance.

$$h = r - \sqrt{R^2 - r^2} \tag{5}$$

$$V = \frac{\pi}{3}.h^2.(3R - h) \tag{6}$$

$$k = \frac{V}{F.L} \tag{7}$$

3 Results

The results regarding the microhardness test shown that a tendency does exist in both the average value and the variation of microhardness throughout the components, however, the value is somewhat different from the reference value that was expected (table 2 and figures 4 and 5).

Table 2. Average microhardness in each tested component.

Component	Microhardness HV
P1 (0,3 mm)	409
P2 (0,9 mm)	547
P3 (0,8 mm)	485
P4 (0,7 mm)	490
P5 (0,8 mm C.C.)	550
W2 (0,9 mm)	282

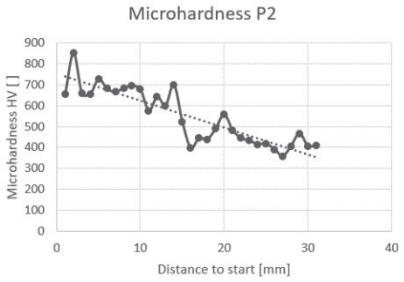

Fig. 4. Microhardness results for component P2.

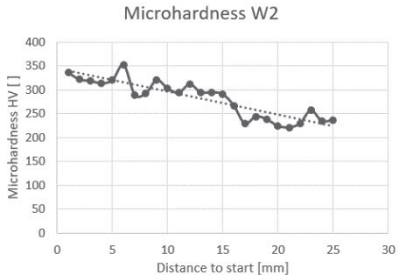

Fig. 5. Microhardness results for component W2.

All of the tested components, both powder and wire LMD, showed a tendency to register higher values of microhardness towards the top of the component (last deposited layers) and lower values of microhardness towards the base of the components (first deposited layers), meaning that throughout the component the value of microhardness tends to decrease.

This decrease of microhardness and its magnitude appears to be related to the layer shift, and consequently to the theoretical layer height, at least on the powder LMD components, given that higher values of theoretical layer height, meant that a steeper variation of microhardness happened from the top of the components to the base of it.

The wire LMD component, despite having a 0,9 mm theoretical layer height, showed a behaviour somewhat approachable to the 0,8 mm theoretical layer height powder LMD variant equivalent, in what microhardness is concerned.

The tendency to register a higher variation of microhardness throughout the component, when higher values of layer shift height are used, is confirmed by the value of the slope of the microhardness tendency lines (Figure 6), which presents a negative value, confirming that the higher values of microhardness are registered near the top of the component, and it also presents a higher absolute value at the higher the layer shift height.

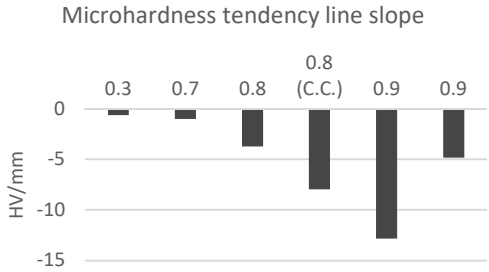

Fig.6. Microhardness tendency line slope, in comparison to the layer shift height.

The test was conducted using deionized water at 20º C, with a corresponding density of 0,99882 kg/m^3 [16]. The mass of the components in dry and submerged state, as well as their density is presented in table 3.

Table 3. Density test results.

Component	Layer shift height [mm]	Mass in dry condition [g]	Mass in submerged condition [g]	Density [kg/m^3]	Variation from reference [10; 11] in %
P1	0,3	6,1624	5,3570	7637,58	2,08% lower
P2	0,7	2,5869	2,2486	7633,00	2,14% lower
P3	0,8	5,6374	4,8938	7567,58	2,98% lower
P4	0,8 CC	7,9109	6,8726	7606,01	2,49% lower
P5	0,9	9,8348	8,5472	7624,34	2,25% lower
W2	0,9	6,4175	5,6157	7989,46	0,01% lower

The density results do not show a clear tendency, with the values for all the powder LMD components being relatively similar, showing that theoretical layer height does not affect density in a significant manner. The wire LMD tested specimens present a density higher than the powder LMD equivalents, however, the difference also occurs because different material was used on both techniques.

Looking at the powder LMD components (P1 to P5) made of Metco 42C, the reference value for density is of 7800 kg/m^3 [11], a value significantly higher than the one registered in the density tests, a tendency that is most likely due to the high porosity.

Regarding the wire LMD component, made with AISI 316L Austenitic Stainless Steel, the registered value is approximately the same as the reference for the material in question, which indicates a lower value of porosity, without significant internal gaps and cracks [11].

The impulse excitation of vibration test was performed on the W2 component, produced by wire LMD, presenting a theoretical layer height of 0,9mm.

The component to be tested was cut to suitable shape, according to the standard, with a length of 54,4±0,22 mm, a width of 17,84±0,026 mm, a thickness of 1,77±0,12 mm and a mass of 12,80 g.

Figure 7 shows both the experimental and analytical vibrational waves that are created when the component was subject to an elastic strike, with a representation of the amplitude of vibration behaviour over time.

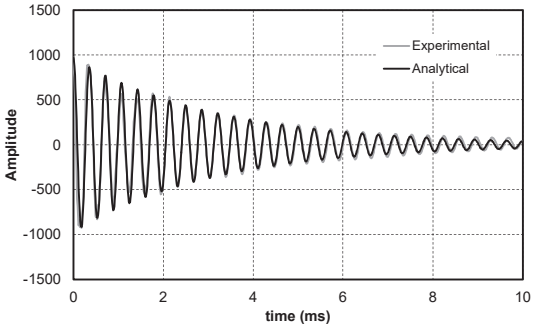

Fig.7. Experimental and analytical response to the impulse excitation of component W2.

Through the representation of the vibration amplitude over the frequency, it is possible to visualize the fundamental resonant frequency, since the highest amplitude is registered within the area of said frequency, much like it is visible in the image below, with the point "1" being the first mode of bending and the point "2" being the first mode of torsion, both obtained by the excitation in different directions.

The frequency at which the first mode of bending is registered is of 2722 Hz and the one at which the first mode of torsion is registered is of 5177 Hz.

With the value presented on figure 8 the mechanical properties are then calculated and the results are presented in the table 4.

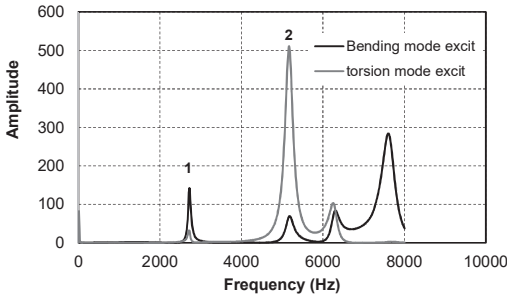

Fig.8. Vibration spectra of component W2.

Table 4. Component W2 mechanical elastic properties, obtained through impulse excitation of vibration testing.

Mechanical property	Value	Variation from reference [11] in %
Young modulus [GPa]	146	24,35% lower
Torsion modulus [GPa]	63,6	17,40% lower
Poisson ratio	0,15	50,00% lower

When comparing the results to the reference values of AISI 316L Stainless Steel, it is possible to register significant differences. This means that the process used to produce this component affects the final mechanical properties significantly.

Some aspects like the thermal cycles suffered by the component during manufacturing as well as the deposition process itself (translation and deposition speeds) end up affecting the material microstructure and the porosity and thus affecting the elastic properties.

The friction and wear test was performed on the W2 component, produced by wire LMD, presenting a theoretical layer height of 0,9mm. The selected component was tested under several wear conditions, under the values of normal force of 3, 5 and 7N, and both the upper portion (last deposited layers) and the lower portion (first deposited layers) of the components also being subject to test. The friction and wear tests were performed at 24 °C and humidity 35 %.

According to the friction test results it is possible to understand that there is a clear relationship between the values of the friction coefficient and the normal load applied to the component during the test, either on the upper part of the specimen or at the bottom. This relationship is established in such a way that when friction coefficient attains a steady state regime, which occurred sensibly within the first 100 seconds of the test, the mean value of friction coefficient was higher for lower normal force values. This relationship can occur due to the wear factor. This means that with the increase of the load it is verified that the wear that occurs in the component is larger, removing a larger quantity of material from the component. Probably, this material is deposited inside the generated crater and most likely will create a tribofilm that provides better sliding conditions between the bodies in contact, which reduces the friction coefficient.

Looking at the variation of the friction coefficient over time (Figure 9), it is possible to identify an initial phase with running-in effect where this coefficient rises rather quickly, until it stabilizes in throughout the rest of the test, at the value of around 0,55. This value should be then compared to the friction coefficient of cast 316L steel under the same conditions, in order to understand how the LMD process affects this parameter.

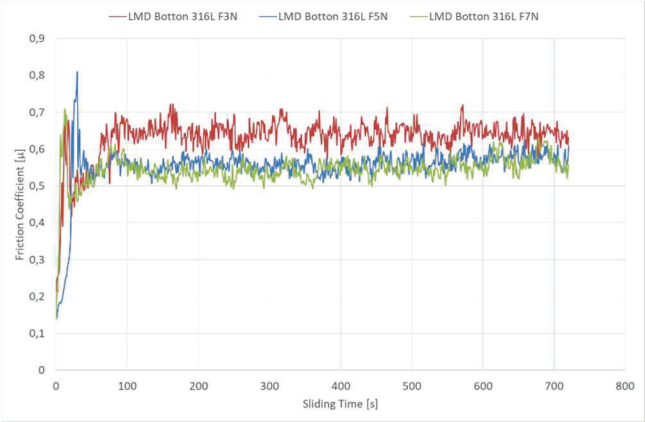

Fig. 9. Friction coefficient during reciprocating sliding tests – lower part.

It should also be noticed that the differences of coefficient of friction observed between the upper and lower part of the component are not significant, only verifying that the measured friction coefficient at the beginning of the test was slightly higher in the case of the lower part of the specimen, however the differences are minimal and do not allow conclusions to be drawn on this aspect.

Another point of interest resultant from the wear test, is the geometry of the wear track itself.

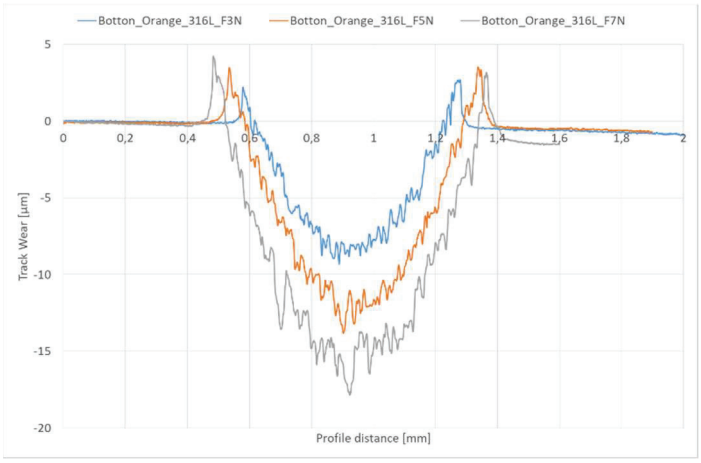

Fig. 10. Cross section profiles from the wear tracks on the bottom portion of the W2 component, for 3, 5 and 7 N of normal force.

With regard to the analysis of the profile of the wear track resulting on the flat specimen it can be verified that there is also a clear relationship between the transverse area of the cavity with the normal force exerted in the specimen during the test.

It is possible to verify that with the increase of normal force there is also an increase in both the profile depth and the profile width (Figure 10).

The results of the upper and lower part of the specimen present a similar tendency and range, with higher values of depth and width of the cavity achieved for a normal force exerted in the specimen of 7N.

All of the wear tests conducted consisted of 1800 reciprocating cycles that ended up in a sliding distance of 7200 mm.

In order to calculate the wear rate coefficient, the diameter of the sphere needs to be calculated, in order to achieve the depth and volume of the wear track.

The Figure 11 in the table 5 presents the wear on the zirconium sphere, where the radius was measured using an image measurement software, named Digimizer. With this data, it was possible to calculate the depth and the volume of the wear scars, using equations (5) and (6), and also the wear rate through equation (7).

Table 5. Zirconium sphere wear scars diameters, depth (*h*) and volume (*V*) of the wear scars, and wear rate (*k*) of the component W2.

	F_N = 3N	F_N = 5N	F_N = 7N
Base portion	d_1 = 597,41 µm d_2 = 688,32 µm h = 10,34e-3 mm V = 16,78e-4 mm^3 k = 7,8e-5 mm^3/N.m	d_1 = 752,43 µm d_2 = 820,47 µm h = 15,49e-3 mm V = 37,65e-4 mm^3 k = 10,5e-5 mm^3/N.m	d_1 = 836,12 µm d_2 = 934,07 µm h = 19,62e-3 mm V = 60,39e-4 mm^3 k = 12,0e-5 mm^3/N.m
Top portion	d_1 = 689,74 µm d_2 = 806,72 µm h = 14,02e-3 mm V = 30,85e-4 mm^3 k = 14,3e-5 mm^3/N.m	d_1 = 792,46 µm d_2 = 823,65 µm h = 16,35e-3 mm V = 41,95e-4 mm^3 k = 11,7e-5 mm^3/N.m	d_1 = 828,58 µm d_2 = 933,75 µm h = 19,45e-3 mm V = 59,35e-4 mm^3 k = 11,8e-5 mm^3/N.m

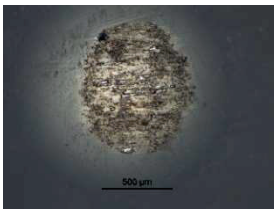

Fig. 11. Wear scar on the base portion of the W2 component, with 7N of normal force.

Comparing the wear rate coefficients, it is possible to identify a difference between the top and base portions, as it was expected given the microhardness variations throughout the vertical axis of the component.

A significant variation between the base and top portions of the specimen was registered especially for the lower values of the normal force, with the top portion registering a wear rate that almost doubles the one registered on the base portion of the component.

This variation should be related to the fact that, under the highest normal load, the pressure is high enough to deform the metallic material closing the porosity, therefore reducing the porosity influence on the wear.

4 Conclusion

The main goal set for this study was the understanding of the main mechanical characteristics offered by components produced with powder and wire LMD.

The microhardness values obtain at the tests decrease from the top of the components to the base (both in powder and wire LMD components), which appears to be related to the theoretical layer height. The wire LMD component tested behaves as the 0,8 mm theoretical layer height powder LMD variant equivalent. Both the tendency hardness gradient and the standard deviation of the microhardness values corroborate the above mentioned conclusions.

It was noticeable that the density of powder LMD components was around 3% lower on all powder LMD specimens, showing that theoretical layer height does not affect the density in a significant manner. With respect to the wire LMD density, similar values were obtained to the reference value, indicating the absence of internal gaps and cracks (low porosity).

By the impulse excitation of vibration test it was possible to conclude that wire LMD component achieved lower results than the reference, namely of Young modulus and Poisson ratio.

The wear test allowed to conclude that the friction coefficient decreases with the increase of normal force used in testing and the wear track geometry is similar for the top

View publication stats

and bottom portion of the components, however, the dimensions tend to be higher on the bottom portion, indicating more wear, possibly due to the lower microhardness. It was noticed that on wire LMD under lower loads (3 and 5 N), the top is much more prone to wear than the base portion. However, at higher loads the tendency shifts and the wear rates between the top and base portion are almost identical.

5 References

[1] Iker Garmendia, J. L. (23-27 de April de 2018). In-process height control during laser metal deposition based on structured light 3D scanning. 19th CIRP Conference on Eletro Physical and Chemical Machining, pp. 375-380.
[2] Benjamin Graf, S. A. (July de 2013). Design of Experiments for Laser Metal Deposition in Maintenance, Repair and Overhaul Applications. 2nd International Through-life Engineering Services Conference, pp. 245-248.
[3] Gary K. Lewis, E. S. (2000). Pratical considerations and capabilities for laser assisted direct metal deposition. Materials and Design 21, pp. 417-423.
[4] Tarak Amine, J. W. (2014). An investigation of the effect of direct metal deposition parameters on the characteristics of the deposited layers. Em H. Qiu, Case Studies in Thermal Engineering (pp. 21-34). Hong Kong: Elsevier.
[5] Stella Holzbach Oliari, A. S. (2014). Additive manufacturing of H11 with wire-based laser metal deposition. Soldagem & Inspeção, pp. 466-479.
[6] Stefan Kaierle, A. B. (2012). Review on Laser Deposition Welding: From Micro to Macro. Physics Procedia 39, pp. 336-345.
[7] Uffe Midtgard, J. E. (1991). Toxicology and occupational hazards of new materials and processes in metal surface treatment, powder metallurgy, technical ceramics, and fiber-reinforced plastics. Scand J Work Environ Health, pp. 369-379.
[8] Vilar, R. (1999). Laser Alloying and Laser Cladding. Materials Science Forum (Volume 301), pp. 229-252.
[9] Hagqvist, P. (5 de July de 2019). Lortek ES. Obtido de Lortek ES: http://www.lortek.es/files/merlin/03-P_Hagqvist-UW&GKN-Aero-Case-study.pdf
[10] Materials, A. (2019). AZO Materials. Obtido de AZO Materials: https://www.azom.com/article.aspx?ArticleID=1023
[11] Steel eagle commerce, l. (2019). Steel eagle commerce ltd. Obtido de Steel eagle malta: https://www.steeleaglemalta.com/grades/
[12] ASTM E92-17, Standard Test Methods for Vickers Hardness and Knoop Hardness of Metallic Materials, ASTM International, West Conshohocken, PA, 2017;
[13] Mazali, I. O. (s.d.). Determinação da densidade de sólidos pelo método de Aqruimedes. LQES - Métodos, processos e técnicas.
[14] ASTM E1876-15, Standard Test Method for Dynamic Young's Modulus, Shear Modulus, and Poisson's Ratio by Impulse Excitation of Vibration, ASTM International, West Conshohocken, PA, 2015;
[15] Amilcar Ramalho, M. D. (2013). Effects of temperature on mechanical and tribological properties of dental restorative composite materials. Tribology International 63, pp. 186-195.
[16] Toolbox, E. (2019). Engineering Toolbox. Obtido de Engineering Toolbox: https://www.engineeringtoolbox.com/friction-coefficients-d_778.html